Salt Effects in the Formation of Self-Assembled Lithocholate Helical Ribbons and Tubes

Pierre Terech,*,[†] Sabareesh K. P. Velu,[†] Petra Pernot,[‡] and Lutz Wiegart[§]

[†]SPrAM, UMR CEA/CNRS/UJF-Grenoble, INAC, F-38054 Grenoble, France
[‡]European Synchrotron Radiation Facility, B.P. 220, F-38043 Grenoble Cedex, France
[§]Photon Division, Building 817, Brookhaven National Laboratory, Upton, New York 11973, United States

Ⓢ Supporting Information

ABSTRACT: The formation of self-assembled nanotubes is usually accounted for by anisotropic elastic properties of membranelike precursors. We present experimental data as evidence of the role played by electrostatics in the formation of self-assembled tubes in alkaline aqueous suspensions of lithocholic acid (LCA). Striking salt effects are characterized by comparing the rheological, dynamical, and scattering properties of systems prepared either in stoichiometric neutralization conditions (SC) of LCA or in a large excess of sodium hydroxide (EOC, experimentally optimized conditions) and finally, in two steps: stoichiometric neutralization followed by an appropriate addition of NaCl (AISC). The SC liquid system is originally made up of loose helical ribbons (previous transmission electron microscopy data), and upon aging they exhibit both intra- and interordering processes. Initially, the helical ribbons are loose and progressively wind around a cylinder ($R = 330$ Å) with their edges exposed to the solvent. They can be temporarily organized in a centered rectangular two-dimensional lattice (*pgg*, $a = 224$ Å, $b = 687$ Å). Upon further aging, the ribbons wind into more compact helical ribbons (or tubes with helical grooves): their edges are less-exposed and their ordering vanishes. Upon addition of NaCl salt (as in the AISC systems), the specific screening of the intra-aggregate electrostatic repulsions induces the closure of the ribbons into tubes ($R_{ext} = 260$ Å, $R_{int} = 245$ Å as in the EOC systems). Simultaneously with the closure of the ribbons into plain tubes, a drastic enhancement of their interconnectivity through van der Waals attractions develops. Eventually, gels are obtained with networks having hexagonal bundles of tubes.
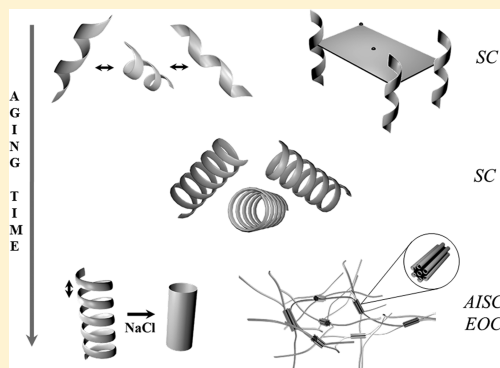
INTRODUCTION

The spontaneous self-assembly of low-mass molecules leading to tubular morphologies is a fascinating field of research, proposing important challenges both in fundamental physics of self-aggregation and in nanoscience applications. Since the pioneering work of J. Schnur[1−4] concerning self-assembled phospholipid tubes, numerous other systems have been discovered, mainly in aqueous solutions that can produce nanotubes.[5] From the perspective of applications in electronics and opto-electronics, the tubular morphology has received particular attention related to the initial discovery of carbon nanotubes.[6] Great effort has been made to obtain similar conductive features via mild conditions of preparation offered by self-assembly processes. In this context, it has been demonstrated[7] that self-assembled tubular systems of amphiphilic coronene derivatives can exhibit very significant electric conductivity. Other applications can be envisaged using chromophoric, template elaboration, or encapsulation properties.[8,9] Biocatalysis and bioseparation applications can also take advantage of the hollow cylindrical structures.[10] Despite the widespread interest in the tubular morphology, its mechanism of formation remains a debated issue.[11] Several theories have evolved in the last three decades, but they do not describe all

structural intermediates that appear during the tubular genesis in a variety of different systems. To date, the theoretical description of the formation of tubes and helical ribbons is based on chiral elastic properties of membranes.[11] The ribbon helicity is driven by the anisotropy of the residual stress in the membrane, in balance with restoring forces induced by elastic bending and stretching.[12] Aside from a description using the chiral elastic properties,[11] other models have been considered based on the electrostatic interactions,[13] elasticity of orientational order,[14] and spontaneous curvature,[15] even if they are not always consistent with current experimental data. In particular, the role of electrostatics in tube formation was the historical approach taken by de Gennes[13] and was discarded as a result of its inability to describe the helical ribbon precursors. A clear dependence of the tube formation on interactions that could be screened by electrolytes was not experimentally observed, and thereby, the electrostatic model was rejected.[16] Interestingly, it has been shown that chiral counterions can be

used to tune the morphology of helical membranes formed by nonchiral Gemini amphiphiles.[17,18]

It has been previously reported that a naturally occurring bile acid, lithocholic acid (LCA), can develop self-assembled nanotubes in aqueous suspensions under alkaline conditions (11.5 < pH < 12.5).[19,20] Scattering and electron microscopy techniques have shown that the formation of the tubes involves not only fibrils and helical ribbons but also coaxial tubes and other structural intermediates, such as short tubes. Little is known about the mechanism of tube formation and the interplay between the different intermediates, and moreover, there is no rationale for defining optimized experimental conditions for their preparation, in particular with regard to the role of electrostatics. We analyze here several preparation options and the corresponding rheological, dynamical, and structural characterizations that shed light on the mechanism of formation of the self-assembled lithocholate tubes. Steroids (like LCA and other bile derivatives) are known to be chiral building units that can be used in unidirectional self-aggregation reactions leading to supramolecular gels.[21] Molecular chirality favors the twist in the molecular orientation and in the associated assemblies but is not a prerequisite to develop chirality in membranelike aggregates. The formation of spiral tubes with chiralities in the micrometer-length scale has been reported[22] in LCA alkaline solutions deposited on glass substrates. Alanine-based amphiphiles can form tubes via helical ribbons whose width and pitch can be sensitive to the cooling rate of the preparations.[23] In the self-assembly of lanreotide octapeptide, different mechanisms for routes followed by the intermediates to tubes have been considered including the closure of helical ribbons.[24] The importance of aging the suspensions has been investigated by cryo-electron microscopy in the chiral self-assembly of a peptidelike molecule and confirms the complexity of the tubular and ribbon geneses.[25] The formation of helical ribbons and tubes, in lithocholate or other mentioned systems, can be interpreted in the context of chiral elastic properties of membranes. Nevertheless, we demonstrate in the present work that electrostatics can also play a crucial role both in the formation of tubes and, ultimately, in the onset of gels. Experimental evidence is given here that the tube and gel formations in lithocholate aqueous suspensions can be very sensitive to the salt content.

■ EXPERIMENTAL METHODS

Lithocholic acid (LCA) (CAS: 434-13-9) was purchased from Sigma-Aldrich (99% purity) and used as received. Typically, 10 mL of a NaOH solution at T_{NaOH} = 0.0266 M was used to dissolve 100 mg of LCA (0.000266 mol) to finally deliver a 1 wt % suspension [SC protocol (stoichiometric conditions)]. One hundred milligrams of LCA (0.00027 mol) was dissolved in 10 mL of a NaOH solution at T_{NaOH} = 0.18 M (0.0018 mol) to deliver a 1 wt % suspension in the EOC (experimentally optimized conditions) protocol. The excess of HO⁻ ions, Δn = 0.00180 − 0.00027 = 0.00153 mol, is replaced by Na⁺Cl⁻ in AISC (adjusted ionic strength conditions) samples. For various calculations used in the preparation of the solutions, the following parameters were used: ρ_{LCA} = 1.121 g cm⁻³,[26] M_{LCA} = 376.58 g mol⁻¹, and ρ_{MeOH} = 0.791 g cm⁻³.

Rheology measurements were performed with a stress-rheometer RS600 (ThermoElectronics) using a cone−plate geometry (radius = 35 mm, 2° angle). A glass cup limited the

water evaporation during the measurements. The temperature was regulated at 20 ± 0.2 °C.

Dynamic light-scattering (DLS) measurements were performed on a Brookhaven BI-200SM goniometer and BI-9000AT digital correlator operating in multi-tau mode, using a He−Ne laser (λ = 632.8 nm operating at 35 mW). The scattered light was collected at a scattering angle of 90° using an avalanche photodiode with an entrance aperture of 100 μm. All measurements were recorded at 25 ± 0.1 °C, and a solvent viscosity of η_s = 0.890 mPa s was assumed. The size distribution of scattered particles was obtained from the analysis of autocorrelation curves by a CONTIN regularization method using the Brookhaven BI-ISDA package.

Viscosimetry measurements have been performed using a Cannon-Fenske viscometer (Comecta) appropriate for New-tonian liquids undergoing a Poiseuille-type flow. The temperature was regulated to 18.6 ± 0.3 °C. The apparatus was calibrated using water and a standard oil (ThermoFisher Scientific) having a 5.3 mPa s dynamic viscosity.

Small-angle X-ray scattering (SAXS) experiments were performed at the ID14-3 beamline[27] at the European Synchrotron Radiation Facility (ESRF, Grenoble, France), using a wavelength of λ = 0.931 Å. SAXS patterns were recorded with a two-dimensional (2D) detector (Pilatus 1M, Dectris), exhibiting a pixel size of 172 × 172 μm², located 2458 mm behind the sample.[28] The isotropic 2D scattering patterns were radially averaged using standard procedures. Anisotropic patterns were averaged by sectors. The range of the scattering vector, Q, was from ca. 0.0045 to 0.5 Å⁻¹ where |Q| = Q = $(4\pi \sin \theta)/\lambda$, where λ is the X-ray wavelength and θ is half the scattering angle. The samples were kept in glass capillaries of a 1.8 mm diameter and 30 μm wall thickness. The 2D SAXS patterns were normalized by the current in the beamstop diode and time per frame prior to radial integration.

The LCA self-assembled species are known to go through various structural intermediates depending on the aging time of the preparation.[19,20,29−31] After a maturation time of ca. 2 days, EOC systems produced tubes as a single population of aggregates. SAXS and rheology experiments are performed on systems (SC, AISC) matured for 4 weeks, unless specified in the text.

■ RESULTS AND DISCUSSION

Lithocholic acid is a secondary bile acid having a single hydroxyl group (at position C-3 of the steroid nucleus) that can be obtained by chemical conversion of the primary bile acids (cholic and chenodeoxycholic).[32] Bile acids are only sparingly soluble in water, and LCA, having a single hydroxyl group, has the lowest solubility of 10⁻⁶ mol/L.[33] Bile salts are soluble amphiphiles with detergent-like properties, and in particular, they can solubilize various lipids. The crystal structure of LCA is orthorhombic, P_{212121} (a = 6.807 Å, b = 12.178 Å, c = 26.779 Å, and Z = 4) showing that all oxygen atoms are involved in hydrogen bonding, accounting for the poor solubility.[26] Studying the LCA behavior[34] in solution is, thereby, difficult due to its poor solubility, and investigations are scarce in comparison to studies of other naturally occurring bile salts such as sodium cholate, deoxycholate, and chenodeoxycho-late.[35] Surface tension measurements[35] suggested that the aggregation process could be more of a continuous association rather than a discrete micelle formation. Nevertheless, curves of the equilibrium surface tension plotted versus bile salt concentration show several discontinuities before the final

Table 1. Preparation Conditions for EOC Systems in Sodium Hydroxide Aqueous Solutions[a]

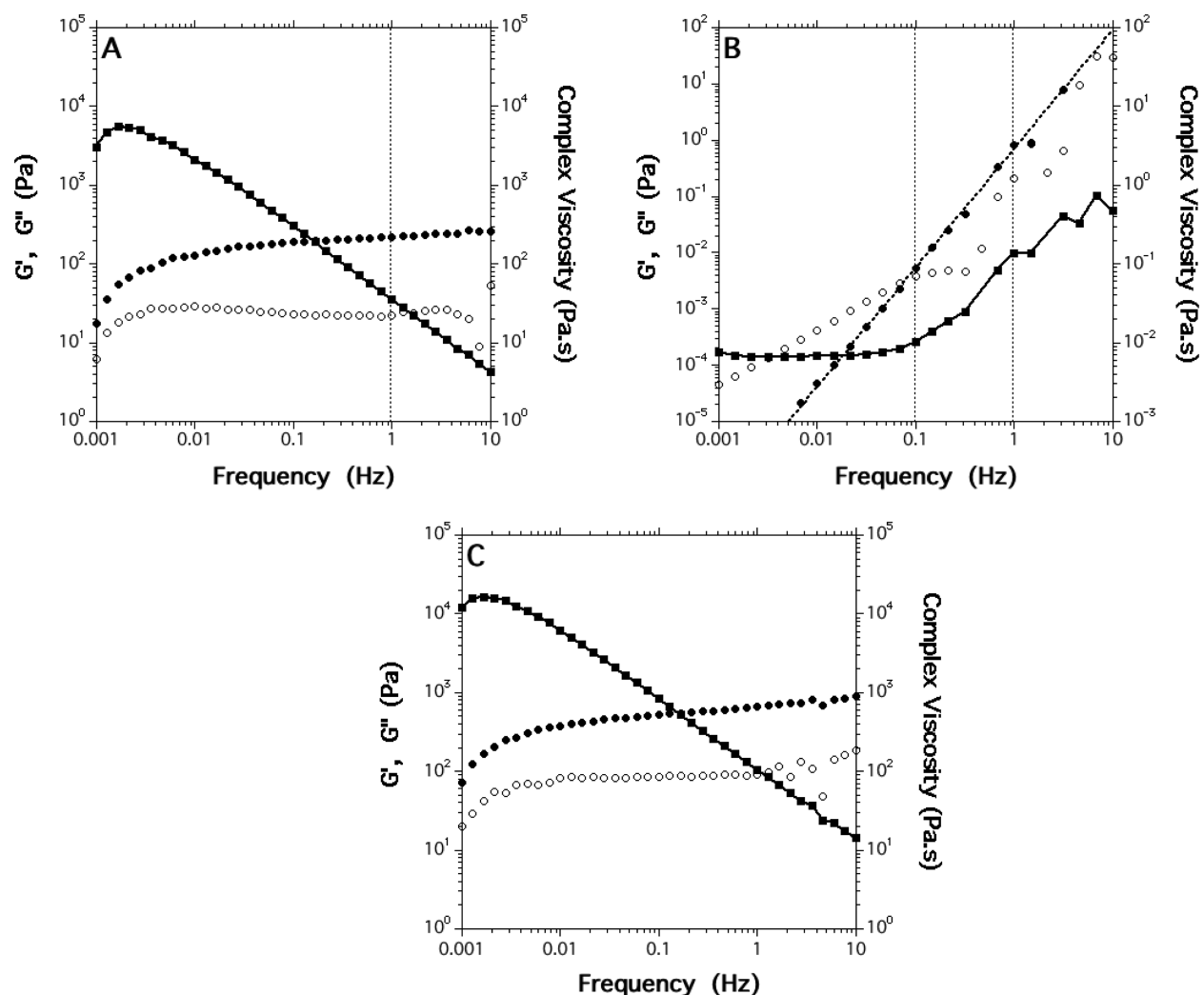| C_{LCA} (wt %)	0.1	0.3	0.5	0.8	1.0	2.0	3.0	4.0	6.0	8.0	10.0
$10^4 n_{LCA}$	0.0266	0.0797	0.1328	0.2124	0.265	0.531	0.796	1.062	1.593	2.124	2.662
T_{NaOH} (M)	0.10	0.13	0.15	0.15	0.18	0.25	0.25	0.25	0.25	0.25	10.0
$10^4 n_{NaOH}$	1.00	1.3	1.5	1.5	1.8	2.5	2.5	2.5	2.5	2.5	10.0

[a]Number of moles n_{LCA} and n_{NaOH} per milliliter are indicated.

Figure 1. Dynamic rheology of 1.0 wt % LCA alkaline suspensions: (●) G′, (○) G″, (■) complex viscosity, η^*. (A) The EOC system where T_{NaOH} = 0.18 M, σ = 1 Pa. (B) The SC system where T_{NaOH} = 0.0266 M. The full straight line is a fit for the complex viscosity (see above). The full line for G″ is a guide for the eye. (C) The AISC system where T_{NaOH} = 0.0266 M + Δn = 0.0018 mol of NaCl.

critical micellar concentration (cmc) is reached. With LCA, such a curve cannot be obtained at pH = 7.0. It was noted that these discontinuities only appear with a small ionic strength and adding electrolytes destabilizes small aggregates, causing them to conglomerate in larger micelles. Typically, the cmc of sodium cholate and deoxycholate is 10.2 and 1.3×10^{-3} M, respectively, at pH = 7.0 in a 0.01 M Na_2HPO_4 buffer solution. In the early 1960s, it was observed by several authors[36−38] that when the pH of solutions of sodium deoxycholate was lowered, the solution became viscous and gels were eventually obtained. The increase of ionic strength partially masks the electrostatic repulsions between the charged bile salt ions, and "micellar" species can grow. A helical arrangement was also characterized with a diameter of 36 Å and a 6.6 Å pitch.[37] The pK_a values distinguish the cholic acid (three hydroxyl groups, pK_a = 5.5)

from the deoxycholic acid (two hydroxyl groups, pK_a = 6.6). It was speculated that the loss of one hydroxyl group was inadequate to explain the pK_a shift. This was later assigned mainly to the formation of helical supramolecules through H bonding between carboxyl groups fixing protons subsequently to a pH decrease. In 1958, Sobotka et al. noticed[38] that the facial amphiphilic nature of bile acids and salts may explain their affinity for lipids. LCA has a single hydroxyl group, and no side of the steroid nucleus is encumbered by polar groups. Thereby, unhindered van der Waals (VdW) attractions can be responsible for the formation of large aggregates. Such a context shows that self-assembly in aqueous bile salt solutions is sensitive to the ionic strength and pH conditions, and helical superstructures can be currently observed. This adds to the

11346

dx.doi.org/10.1021/jp305365m | J. Phys. Chem. B 2012, 116, 11344−11355

relevancy of the present investigation concerning the role of electrostatic conditions for the formation of lithocholate tubes.

Previous studies on LCA have shown that long (length $L > 1$ μm)[31] tubular species with monodisperse cross sections are formed at high pH values of the aqueous suspensions. SAXS measurements and cryo-transmission electron microscopy (TEM) micrographs give similar values for the external diameter, D_{ext} (520 Å), and the cylindrical internal cavity, D_{int} (490 Å).[19] The neutralization was performed with NaOH or NH$_4$OH, and significant effects of the counterion type (Na$^+$ vs NH$_4^+$) on the radial polydispersity and ability to form oriented bundles were revealed.[39] In particular, it has been observed that for concentrations $C \geq 7.9$ wt %, bundles of hexagonally packed tubes develop in the junction zones of gel-like phases. Up to now, the recipe for the preparation of lithocholate tubes has been based on the alkali concentration delivering the highest rigidity and optical transparency of the gel-like samples (for $C > 0.5$ wt %).

Alternatively, the preparation of concentrated samples was optimized using a microscopic observation with crossed polarizers. No heating was used to avoid any disruption, dissolution/micellization reactions, or phase transitions in the systems.[20] Table 1 shows the preparation conditions for EOC samples. The overlap threshold of the species formed in an excess of NaOH ($T_{NaOH} = 0.12$ M) can be determined by viscosity measurements. A capillary viscometer is used (see S1 of the Supporting Information) to extract $C^* \sim 0.5\%$. Beyond this threshold, a sharp enhancement of the viscosity is assigned to a sharp increase of interactions. In the present contribution, comparisons between different systems are made for concentrations larger than C^*: with EOC and AISC (vide infra), gels are obtained.

Other preparation protocols can be considered. SC systems are those for which LCA and NaOH molarities are identical. Table 1 shows that in EOC systems, a large excess of sodium hydroxide is used. It turns out that a new type of protocol can be considered where the excess HO$^-$ ions (Δn) of the EOC systems can be replaced by NaCl ions (AISC). We thus focus on these three types of systems: EOC, SC, and AISC. It is expected that the different protocols, which involve different ionic-strength conditions, will affect the morphology and/or the level of connectivity of the aggregates. Small-angle X-ray scattering, dynamic light scattering, and rheometry techniques are therefore suitable for such an investigation.

Figure 1 shows strikingly different rheological behaviors for EOC, SC, and AISC systems. The reference EOC system (C_{LCA} = 1 wt %, $T_{NaOH} = 0.18$ M) behaves like a gel on a short time scale since the ratio of the elastic over the loss moduli is G'/G'' ≈ 10 (Figure 1, panel A). For $\nu = 0.001$ Hz, G'/G'' is reduced to 2.8, suggesting that over long periods of time, the system may flow due to the existence of slow relaxation modes. This behavior differs notably from that of "ordinary" molecular gels prepared from low-mass molecules (gelators) that exhibit a constant G'/G'' ratio over the whole frequency range (between 10^{-4} and 100 Hz).[21] The SC system (Figure 1B) exhibits a very different G', G'' versus frequency profile, showing much smaller absolute values. At $\nu = 1$ Hz, $G'/G'' \approx 3$ with G' (1 Hz) ≈ 0.7 Pa, whereas for EOC, G' (1 Hz) ≈ 218 Pa. Interestingly, $G'(\nu)$ and $G''(\nu)$ curves coincide ($G' = G''$) at $\nu = 0.1$ Hz. At low frequencies ($\nu < 0.1$ Hz), the elastic shear modulus $G'(\nu)$ exhibits a slope of $0.7\nu^{2.1}$, while the loss modulus, $G''(\nu)$, varies as $0.7\nu^{1.2}$. Such slopes at low frequencies are typical for a liquidlike material for which theoretical exponents of the

dynamic rheology are 2 and 1,[40] respectively. At $\nu < 0.1$ Hz, the SC system is a Newtonian liquid exhibiting a plateau of complex viscosity ($\eta^* = 11$ mPa s) in the lowest-frequency domain. Beyond $\nu = 0.1$ Hz, the viscosity is increasing and G', G'' follows a quadratic law with ν and a ratio of $G'/G'' \approx 2-3$ revealing weakly interacting species.[41]

Finally, the SC systems are prepared via a complete neutralization reaction of the weak acid LCA by the strong alkali NaOH. The flow properties of the SC ionic aggregates reveal their much weaker interaction potential (compared with EOC systems). The excess HO$^-$ ions (Δn) from the SC to EOC systems thus appear determinant in the mechanism of formation of the tubes and/or their interactions. In the AISC systems, this excess is replaced by NaCl (Δn). The resulting rheological profiles (Figure 1C) now appear similar to those in Figure 1A for the EOC systems. Since the acid-to-salt conversion is assumed to be complete, it is reasonable to assume that the number density of aggregates (whatever their form factor) is similar in the SC, AISC, and EOC systems, but their level of interaction is greatly different. In particular, the connectivity in the AISC and EOC systems is considerably larger than in the SC liquidlike systems.

Dynamic light-scattering measurements[28] on fresh SC systems confirm the presence of weakly interacting aggregates (with a measurable size) compared to the AISC and EOC systems. Figure 2 displays the normalized time-averaged
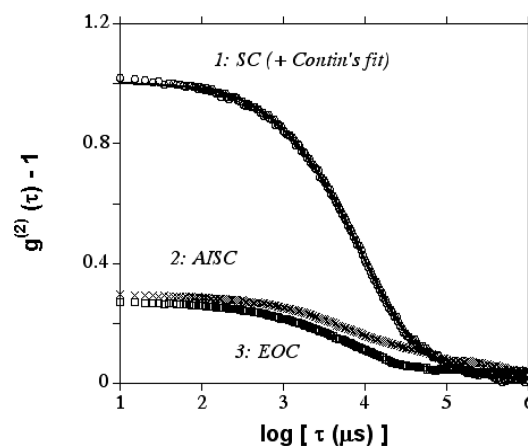

Figure 2. Normalized time-averaged intensity−intensity autocorrelation functions for the fresh SC, equilibrated EOC, and AISC systems. Experimental data are the symbols, and the solid line is the CONTIN fit.

intensity−intensity autocorrelation function $g^{(2)}(\tau)$ for SC, AISC, and EOC systems. It can be clearly noted that for SC, the zero-time amplitude $[g^{(2)}(\tau = 0) - 1]$ decays from approximately one to zero, revealing the ergodic behavior (fluidlike) of the system, such that the scatterers (aggregates) are highly delocalized and evolve through all of the possible spatial configurations. The AISC and EOC systems show a reduced zero-time amplitude indicating the nonergodic behavior as observed in gel-like[42] systems: the scatterers become more localized and fluctuate about their mean position only. This behavior is interpreted as being due to the strong interactions between the aggregates, making them localized, and thus able to form gel-like systems. For the ergodic sample SC, the measured normalized time-averaged intensity−intensity autocorrelation function, $g^{(2)}(\tau)$, at a given scattering wave

vector, $Q = (4\pi n/\lambda) \sin(\theta/2)$ (where n is the refractive index of the medium, λ is the wavelength of the incident laser beam, and θ is the scattering angle), is given by eq 1:[28]

$$g^{(2)}(\tau) = \frac{\langle I(q, t + \tau)I(q, t)\rangle}{\langle I(q, t)\rangle^2} \quad (1)$$

The time-averaged $g^{(2)}(\tau)$ is related to the time-averaged electric field autocorrelation function, $g^{(1)}(\tau)$, through the Siegert relation (eq 2):

$$g^{(2)}(\tau) - 1 = |\beta g^{(1)}(\tau)|^2 \quad (2)$$

The coherence factor, β (≤ 1), depends on the experimental setup. When the scattering species are monodispersed, $g^{(2)}(\tau) - 1$ can be fitted to a monomodal distribution (single-decaying exponential function) with a characteristic decay rate ($\Gamma = DQ^2$), where D is the diffusion coefficient of the scattering species. For polydisperse species, the mean characteristic decay rate ($\langle\Gamma\rangle = \langle D\rangle Q^2$) can be obtained by using a nonmonomodal distribution function such as the CONTIN regularization function[43] (solid line of the SC sample). Knowing $\langle D\rangle$, the mean hydrodynamic radius, $\langle R_H\rangle$, can be calculated using the Stokes−Einstein relation.[33] The mean translational diffusion coefficient measured for SC is 2.28×10^{-9} cm^2/s, and the corresponding hydrodynamic radius of the aggregates is 1.07 μm (polydispersity = 1.84). For AISC and EOC, due to the nonergodic character of the systems, analyzing the time-averaged autocorrelation functions becomes more complex. However, the measured $g^{(2)}(\tau) - 1$ for the AISC and EOC samples suggests that they are gel-like systems with similar aggregates in form, number density, and level of interaction.

Among various scenarios that can account for the experimental findings, those implying an interplay between electrostatic and van der Waals interactions in a "living" chiral self-assembled system have to be considered. Obviously, the balance of interactions can be tuned by addition of salt. In this respect, an investigation of the kinetics of the flow evolution of AISC just after salt injection can be instructive. Figure 3 shows that the profile for EOC is strikingly different from that for AISC. The equilibration of the viscosity in the reference EOC system is much faster (curve 1) than in the SC system, to which NaCl is added so as to form AISC (curve 2). The viscosity tends to evolve toward the equilibration value in EOC. The relatively short characteristic time for equilibration in curve 1 is assigned to the orientational relaxation at low shear (dγ/dt = 0.01 s^{-1}) of the tube suspension after its introduction in the gap of the rheometer. The much slower (at least 2 orders of magnitude) equilibration observed in AISC (curve 2) suggests that major morphological and/or connectivity modifications are occurring in unfavorable diffusion conditions.

To further characterize the interactions in AISC and EOC gels, the mechanical stress relaxation function can be approached by creep-recovery measurements. This will indicate if the two systems are completely identical. First, the reference system EOC at 1 wt % is analyzed and good quality fits of the creep and relaxation segments are shown in Figure 4 (panels A and B), while results for AISC are shown in Figure 4 (panels C and D). The creep parts (Figure 4, panels A and C) can be modeled by eq 3 describing the behavior of a series association of Maxwell and Kelvin−Voigt elements. It is known as the Burgers model frequently used in polymeric or surfactant materials[35] and can combine relaxation and retardation phenomena in a single material.
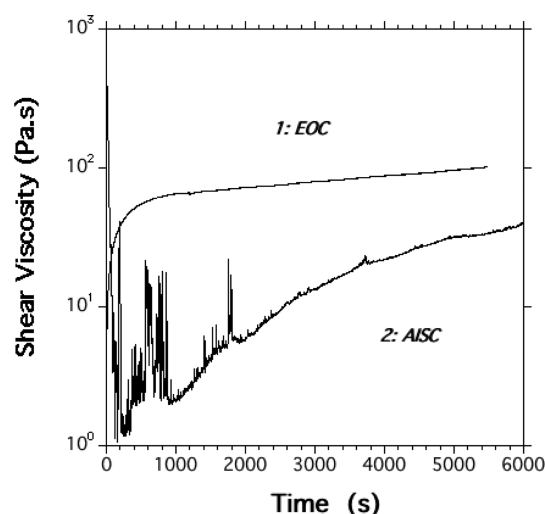

Figure 3. Viscosity of a 1 wt % LCA alkaline aqueous system at a shear rate of 0.01 s^{-1}. Curve 1: The reference EOC sample. Curve 2: The AISC sample was introduced into the gap immediately after the NaCl addition. The origin of the viscosity spikes in the first stages of the kinetics is related to the mode of salt introduction. Addition in the solid form generates microgels around the grains, while an introduction in a dissolved liquid state is more homogeneous and minors these erratic features.

$$\gamma(t) = \gamma_M + \frac{\sigma_0}{G_K}(1 - e^{-t/\tau}) + \frac{\sigma_0 t}{\eta_M} \quad (3)$$

with $\tau = \eta_K/G_K$, where η_K and G_K are the viscosity and shear modulus of the Kelvin element, respectively; γ_M and η_M are the instantaneous deformation and viscosity of the Maxwell element, respectively. The creep part has three components: instantaneous elastic deformation σ_0/G_M, delayed elastic deformation $\sigma_0/G_K[1 - e^{-(t/\tau)}]$, and viscous irreversible deformation $(\sigma_0 t/\eta_M)$.

The total deformation is mathematically described by a linear superposition of the above components. From the rheological equation $\gamma(\sigma)$ of the Burgers model, the relaxation behavior is obtained as a solution of the second-order differential equation as in eq 4.

$$\sigma(t) = C_1 \exp\left(-\frac{t}{\theta_1}\right) + C_2 \exp\left(-\frac{t}{\theta_2}\right) + C_3 \quad (4)$$

where θ_1 and θ_2 are two independent relaxation times.

The quality of the fits is identical for the two classes of systems, EOC and AISC, guaranteeing meaningful comparisons. The parameters used for fits according to eqs 3 and 4, the fraction of instantaneous and delayed elasticity, and irreversible deformation are listed in Tables 2 and 3.

The high proportion of the irreversible recovery is a common feature of molecular gels whose linear elastic domain is usually small (typically $\gamma < 0.01$). Here, an order of magnitude in the amplitude of deformation distinguishes AISC and EOC systems (Figure 4). Both systems creep with a similar characteristic time, but with AISC the viscoplasticity is larger by 2 orders of magnitude and deforms accordingly. The network of interacting aggregated species in AISC gels is more fragile and labile than in EOC gels. The instantaneous elastic recovery in AISC gels is diminished while the irreversible part is increased. This indicates that even if gels appear macroscopically similar, in terms of shear elasticity, the cohesiveness in AISC is
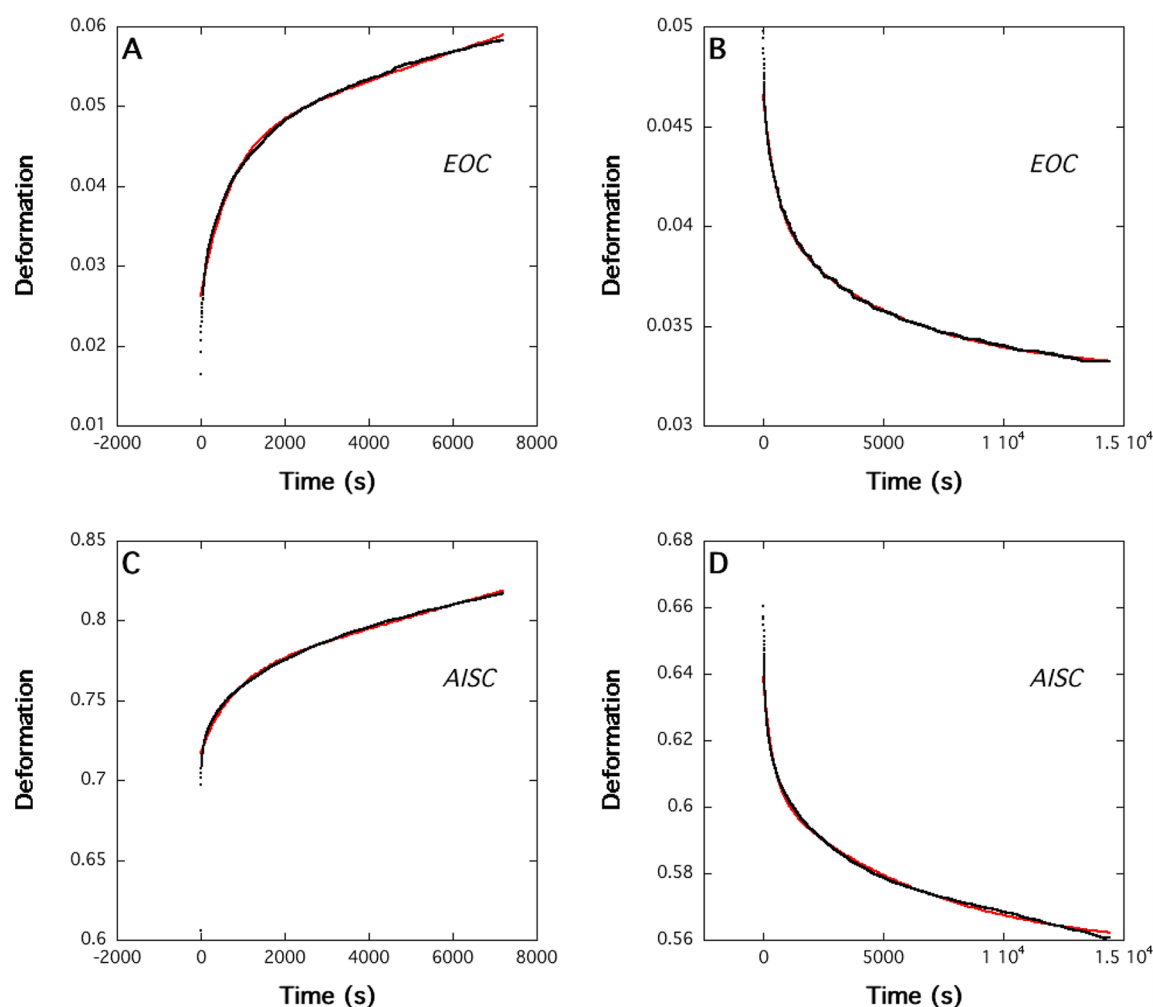
Figure 4. Creep-recovery measurements of an EOC system (C_{LCA} = 1.0 wt %, top line) and AISC system (C_{LCA} = 1.0 wt %, T_{NaOH} = 0.0266 M, + Δn NaCl bottom line) gel. Creep segments (left column): (A and C) fit according to eq 3. Relaxation segments (right column): (B and D) fit according to the biexponential decay of eq 4. Fits (red full lines) and data (black dots) are hardly distinguishable. Parameters are summarized in Tables 2 and 3.

Table 2. Creep Segments in Figure 3 (Panels A and C)[a]

creep	τ (s)	G_K/σ_0	G_M/σ_0	σ_0/G_M elastic	$\sigma_0/G_K[1 - e^{-(t/\tau)}]$ viscoelastic	$(\sigma_0 t)/\eta_M$ viscoplastic
EOC	726	50	16	0.18×10^{-5}	0.02	0.18
AISC	770	20.7	1.4	0.74×10^{-5}	0.048	18.3
AISC/EOC ratio	1.1	0.41	0.09	4.1	2.4	102

[a]Best fits following eq 3. Viscoelastic and viscoplastic components are calculated for $\Delta t = 10^5$ s.

Table 3. Relaxation Segments in Figure 3 (Panels A and C)[a]

recovery	C_1 (Pa)	θ_1 (s)	C_2 (Pa)	θ_2 (s)	C_3 (Pa)	elastic (%)	delayed (%)	irreversible (%)
EOC	0.00778	5457	0.0061	543	0.03268	13	17	70
AISC	0.0487	6562	0.0336	394	0.5568	5	8	87
AISC/EOC ratio	6.3	1.2	5.4	0.73	17	0.4	0.5	1.3

[a]The three last columns are calculated from best fits using eq 4 at limiting conditions (time = 0, small, and infinite).

considerably weakened by the two-step protocol. The formation of chiral ribbons and their time evolution in EOC appear to be the most appropriate electrostatic conditions for optimizing the connectivity of the species. Restrictions in the diffusive motions of the species in SC diminish the proportion of junction zones in the resulting elastic network. These results illustrate the striking influence of salt addition on the flow properties. This is confirmed with creep-recovery experiments involving increasing NaCl amounts, from a nearly SC system[a]

to a AISC (Supporting Information, Figure S2). The amplitude of deformation is strongly diminished (by more than an order of magnitude) when salt is added.

Salt effects can also be seen by the variations in the viscosity profile as a function of added salt in a specific shear protocol made up of two segments. The first segment is an imposed creep at $d\gamma/dt$ = 300 s^{-1} for 600 s immediately followed by an ascending shear rate ramp from 0 to 400 s^{-1}. The preshearing segment allows a better reproducibility of the experiments since
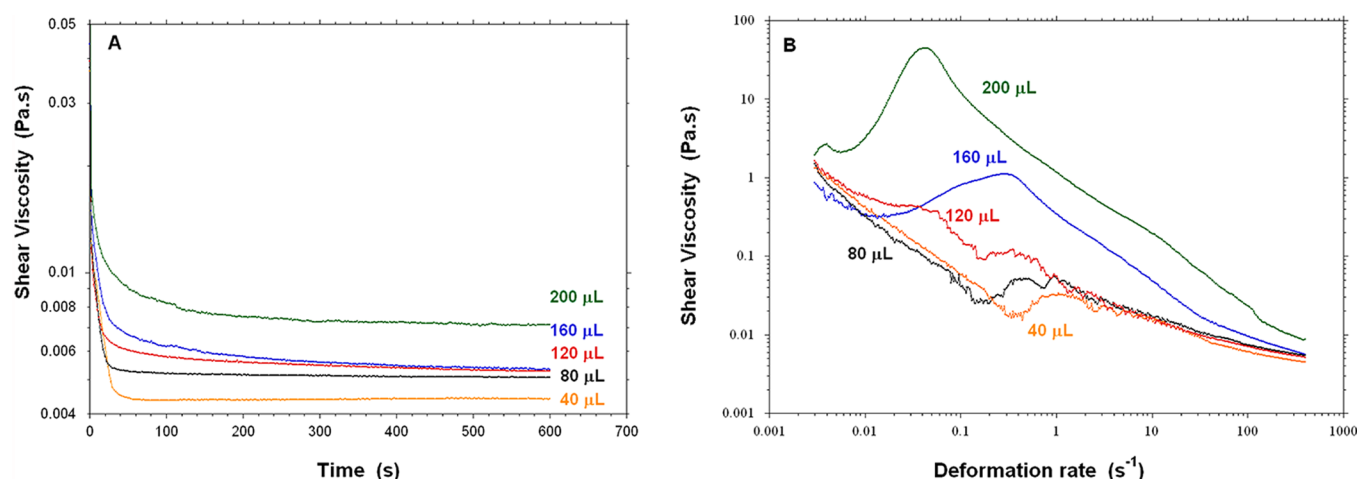
Figure 5. Shear viscosity variations in an alkaline solution of LCA ($C = 1.0$ wt % in $T_{NaOH} = 0.0266$ M) and increasing amounts of NaCl (40, 80, 120, 160, and 200 μL of a solution at $T_{NaCl} = 3.83$ M). (A) Creep segment at $d\gamma/dt = 300$ s^{-1}. (B) Flow curves.

all systems undergo the same rheological history. Figure 5A shows that the viscosity amplitude at equilibrium follows the sequence of increasing salt amounts ($T_{NaCl} = 3.83$ M). Figure 5B shows a similar tendency for the flow curves. In addition, the profile is complex with shear-thickening overshoots in the most salted samples (200 and 160 μL of added NaCl solution). Small amounts of salted solution are sufficient to initiate the progressive onset of viscoelasticity. These features confirm that the interaction level of the charged self-assembled species is increasing by adding salt. The viscosity overshoots are assigned to further transient aggregations (bundles) in a shear-induced context.

The SAXS experiments using a synchrotron source are then conducted to decipher the structural origin of the observed rheological differences. Curve 1 of Figure 6 shows the scattering curve of the EOC reference system. It is known[31] to be typical of a suspension of nanotubes with an external diameter of 520 Å and an internal cavity of 490 Å. In the present preparation and scattering conditions, up to 10 intensity oscillations are observed and mainly assigned to form-factor contributions.[39]
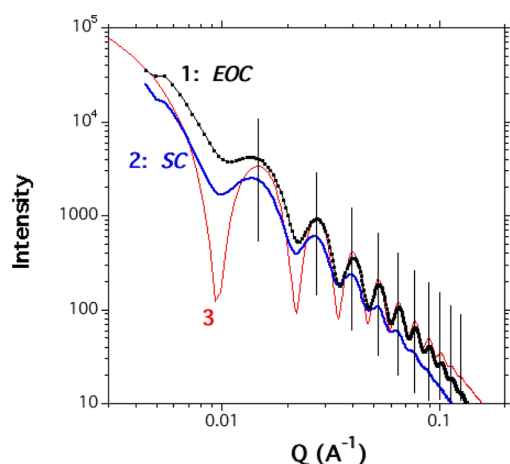

Figure 6. SAXS of LCA systems at $C_{LCA} = 1$% wt in alkaline aqueous solutions. Curve 1: EOC ($T_{NaOH} = 0.18$ M); Curve 2: SC ($T_{NaOH} = 0.0266$ M). Curve 3: indicative theoretical form-factor scattering function (eq 5) with $R_{ext} = 260$ Å, $R_{int} = 245$ Å, and $\varepsilon = 0.05$. Vertical bars indicate the 10 form-factor oscillations (see text).

Curve 3 shows an indicative theoretical form-factor scattering profile (eq 5) for long tubes whose internal cylindrical cavities are filled with the same surrounding medium.

$$I(Q) = \left\{ \frac{\pi L[2A(\rho_{ext} - \rho_{int})]^2}{Q} \right\}$$
$$\left\{ \left(\frac{\rho_{ext} - \rho_{sol}}{\rho_{ext} - \rho_{int}} \right) (R_{ext}{}^2) \left[\frac{J_1(QR_{ext})}{QR_{ext}} \right] - R_{int}{}^2 \left[\frac{J_1(QR_{int})}{QR_{int}} \right] \right\}^2$$
(5)

J_1 is the Bessel function of the first kind. R_{ext} is the external radius, and R_{int} is the internal radius of the tube (annular cross section A and length L). ρ values are the electronic densities expressed in e Å^{-3}. Equation 5 simplifies whether the internal cavity of the tube is filled with the same surrounding liquid ($\rho_{int} = \rho_{sol}$). The effect of the length $\langle L \rangle$ is not considered in matured EOC systems since previous cryo-TEM measurements[44] have shown only long tubes (>1 μm).

The SAXS of a matured SC liquid suspension shows a number of scattering features comparable to those of EOC. Nevertheless, only seven less-pronounced oscillations (Figure 6, curve 2) can be observed. This curve indicates that the structure of the scattering species in SC is closely related to the tubular morphology. Previous cryo-TEM studies[36,20] of EOC systems have shown both loose and tight helical ribbons, as well as the short tubes preceding the formation of the longer tubes. A scenario that can be envisaged considers loose and charged helical ribbons wrapping into more compact helical ribbons (reducing their pitch, P) resembling the final tube morphology (i.e., almost a closed tube or a tube with a helical groove). A second scenario could consider short tubes in SC that, upon appropriate electrostatic screening of their exposed ends, would paste to increase their lengths and thereby overlap in gel phases. Theoretical SAXS modeling does not support this option. Indeed, the corresponding scattering function separates the axial and cross-sectional terms and affects only the low-angle part of the scattering profile for an angular range corresponding to the contour length of the short tubes (see S3 of the Supporting Information).[20] In addition, the mechanism for the formation of helical ribbons from rolled membranes shows that the 2D spatial extension of these later determines in turn the length and width of the curling ribbon. It is important to note that interacting helical aggregates do not optimize van
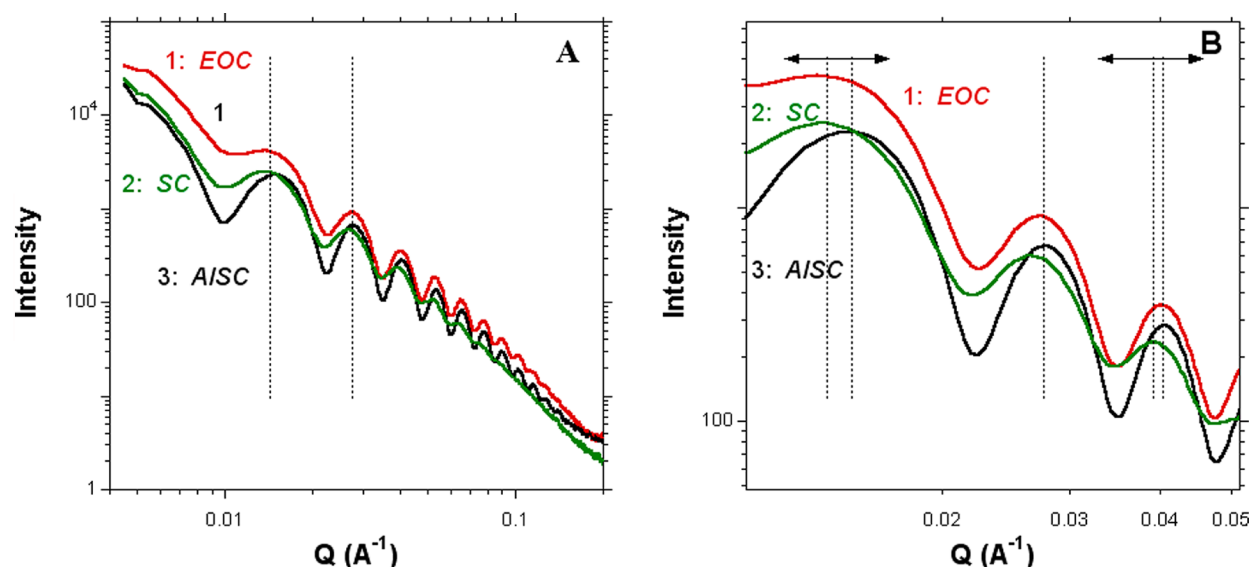
Figure 7. SAXS of LCA alkaline aqueous systems at $C_{LCA} = 1\%$ wt. Curve 1: EOC prepared in $T_{NaOH} = 0.18$ M. Curve 2: SC prepared in $T_{NaOH} = 0.0266$ M. Curve 3: AISC prepared in $T_{NaOH} = 0.0266$ M + 120 μL of 3.83 M NaCl. (A) The three systems show very comparable oscillations, and (B) is an enlargement of the first three oscillations.

der Waals attractions as plain tubes can do. The sol-to-gel transition is induced by a proper addition of salt, from SC to AISC systems. The addition screens specific electrostatic repulsions and, in turn, amplifies VdW attractions. The exposed and charged edges of the ribbons can undergo electrostatic interactions triggered by the ionic strength of the embedding medium. In particular, intra- and interordering processes can sophisticate the time evolution of chiral ribbons. To illustrate, fresh SC systems are made up of freely diffusing long species as shown by the present DLS experiments. Such species can be loose helical ribbons as shown by already mentioned previous cryo-TEM experiments. Upon aging, the ribbons strongly interact and organize in a centered rectangular lattice *pgg* (interordering, see Appendix). After further aging ($\Delta t < 4$ weeks), the ribbons wrap to tighter chiral morphologies with reduced P (intraordering): the diameter is kept constant, but the ratio pitch/R is reduced. Equivalently, the width of the helical groove on the winding cylinder is reduced. The charged edges of the ribbons become buried in the morphology and consequently, their direct interactions vanish as well as their interordering. The SAXS of equilibrated SC systems (3 weeks) indicates that the scattering species are structurally closely related to the tubular morphology (helical ribbons) in a liquidlike system.

Figure 7 (panels A and B) shows the variations of the AISC scattering curves when NaCl is added to the SC samples so as to reach the concentration conditions of the EOC systems. Assuming that all LCA is converted into carboxylate anions in the SC systems, the operation thereby describes the role of Cl$^-$ anions. Rheological measurements have shown that the added salt induces a sharp increase of elasticity up to values usual for EOC systems. Nevertheless, the cohesiveness or resistance to creep of the AISC networks remains weaker.

The SAXS profile of AISC is shown in Figure 7 and exhibits marked oscillations located at the same Q positions as those of EOC. At this stage, it can be claimed that tubes found in EOC are also present in AISC. The intensity at low Q for SC and AISC is diminished compared to that of EOC; it reveals the influence of interference between the species (structure factor).

This is qualitatively consistent with the scenario of electrostatic interactions (intra- or interaggregate) between exposed edges of helical ribbons that do not exist with plain cylinders in EOC systems. The buckling (intra-aggregate mechanism) of the ribbon edges can be triggered by the salt content, while the bundling of the subsequent tubes (interaggregate mechanism) results from the enhanced VdW attractions when the helicity is lost. Indeed, the attraction between twisted fibrils is much weaker than between cylinders and is maximal for straight, oriented cylinders.[45] Figure 7B also shows a small large-Q shift from SC to EOC ($Q_{SC} = 0.0266$ Å^{-1}, $Q_{EOC} = 0.0275$ Å^{-1}) which will be explained below. The evolution from loose helical ribbons to more compact ones and finally to plain tubes by closure of the helical groove can be illustrated by SAXS. Various theoretical models are available to describe helical morphologies,[46,47] and the Schmidt's model[48] is used here for its convenience and versatility. The circular section of the helical morphology is sketched by sectors extending from the center with variable angular and radial extensions. The model covers the cases of single, double, and hollow helices and can be extended to ribbons. To summarize

$$QI(Q) = \sum_{n=0}^{\infty} \left[\varepsilon_n \cos^2(n\phi/2) \right] \left[\frac{\sin^2(n\omega/2)}{(n\omega/2)^2} \right] \left[g_n(QR_{ext}, R_{int}) \right]^2 \quad (6a)$$

where R_{ext} is the external radius of the helix and R_{int} the hollow part.

$$g_n(QR_{ext}, R_{int}) = (2R_{ext}^{-2})(1 - R_{int}^2)^{-1} \int_{R_{ext}R_{int}}^{R_{ext}} rJ_n(Qr\sqrt{1 - q_n^2})dr \quad (6b)$$

with $b = 2\pi R_{ext}/P$, $q_n = nb/QR_{ext}$, $QR_{ext} \geq nb$,

$$q_n = 1, \quad QR_{ext} \leq nb, \quad \varepsilon_0 = 1\varepsilon_n = 2n \geq 1 \quad (6c)$$

ω is the angular of the sector of material, φ is the angle between the two sectors of a double helix, and P is the helix period. The number of terms in the summation is limited to terms for $n \leq QR_{ext}/b$. To illustrate, this model has been used with a steroid molecular organogel[49] and in the nanotube formation of hexa-perihexabenzocoronene-based molecules.[50] Figure 8 shows
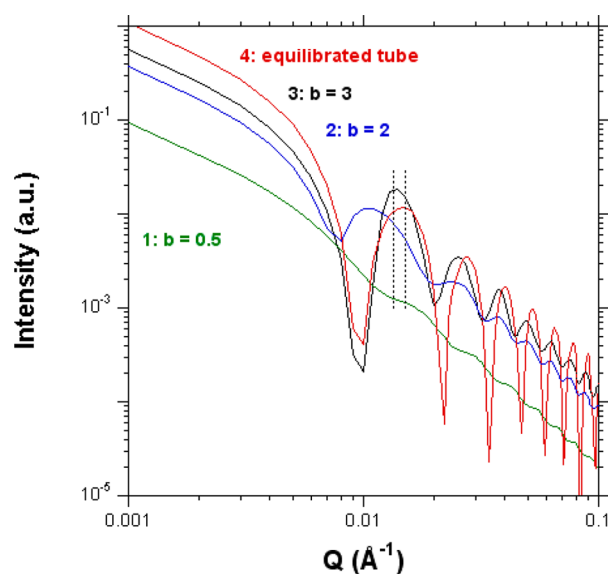

Figure 8. From loose helical ribbons to plain tubes, SAXS modeling follows eqs 6a−6c (ω = 3 rad, R_{ext} = 260 Å, R_{int}/R_{ext} = 0.942, φ = 0). Increasing b values ($b = 2\pi R_{ext}/P$) lead to similar scattering profiles.

theoretical scattering profiles according to eqs 6a−6c, for more or fewer loose ribbons in reference to the scattering of tubes as those found in EOC samples. Parameters used to model the present structural scenario from helical ribbons to tubes are then single helicity (φ = 0), $R_{ext}(1 - R_{int}/R_{ext})$ defining the thickness of the ribbon while ω is made similar to their width.

Figure 8 shows that, by contrast to tubes, loose ribbons do not exhibit pronounced form-factor oscillations which make their detection by SAXS difficult. Here, previous cryo-TEM experiments have shown their existence in the first stages of the tubular genesis. As the helical ribbon becomes more compact (b increases and the pitch reduces), oscillations are more resolved and approach the positions corresponding to the final tube (the diameter of the virtual tube on which the ribbon winds is kept identical). Interestingly, for the last step (curve 3 in Figure 8) where only a thin helical groove decorates the tube, oscillations are slightly low-Q shifted and smoothed. These theoretical observations correspond to the present experimental data (*vide supra*) and support the hypothesis of the mechanism of closure of the ribbon into tubes by a fine screening of the electrostatic interactions using salt addition.[b]

Figure 9 is a naive illustration of the structural genesis of loose ribbons whose exposed edges interact to order in a rectangular symmetry. When the ribbon ages, the morphology of the helical ribbon condenses progressively (P diminishes) and the suspension randomizes. Later on, the helical grooves in the AISC systems collapse on appropriate salt addition, and plain tubes are formed. The fine electrostatic screening allows the VdW attractions to overwhelm the interactions, and gels with hexagonal bundles can be formed. The steps are in phase
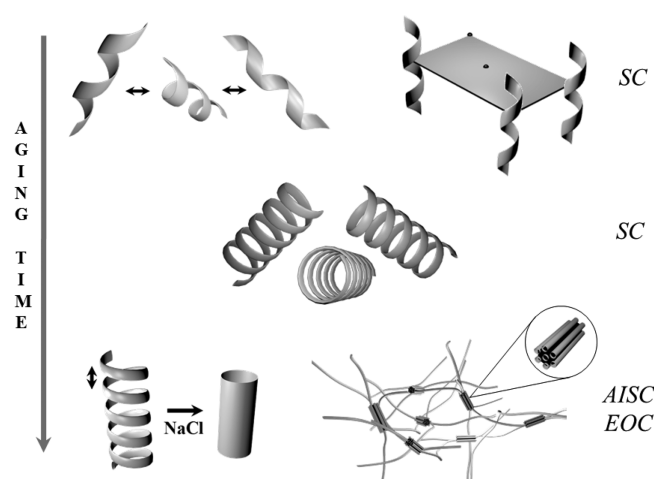

Figure 9. Structural sequence of the tubular formation in the LCA systems (SC, AISC, and EOC) as a function of aging time and salt concentration. First line: loose ribbons interact and order into a *pgg* 2D symmetry (double arrows point at intra-aggregate electrostatic interactions). Middle line: the helical ribbons become more compact, and the ordering vanishes. Bottom line: almost closed helical ribbons (as in SC) can collapse into plain tubes as in AISC (double arrow indicates interaggregate interactions). They interact through VdW interactions in gels with *p6m* ordering in the bundles as in EOC.

with a maximal efficiency in EOC systems and sequential and less-optimized in AISC systems.

Despite the fact that the role of electrostatics in tube formation[13] was neglected in the theoretical literature (see Introduction) due to a lack of experimental evidence,[11] we demonstrate here that it can play a determinant role with lithocholate systems. Tube and gel formations can be made salt-sensitive in a special two-step preparation protocol. The first step considers stoichiometric neutralization conditions delivering loose helical ribbons. The species are "living suprapolymers" evolving upon aging toward tubes decorated with helical grooves that can be further collapsed to plain tubes and gels by a suitable salt addition. At this stage, it is instructive to consider in more detail the titration of LCA by a sodium hydroxide solution.

As mentioned above, the poor solubility of LCA in water prevents such a neutralization reaction from being performed in a homogeneous aqueous phase. LCA is soluble in methanol or ethanol, but there is no macroscopic evidence (viscosity, birefringence) that once LCA is neutralized in alcoholic medium, tubes can be formed. It has also been supported by SAXS for which the alcoholic solutions do not exhibit any scattering signal aside from the diffuse scattering from the liquid (not shown). Figure 10 (curves 1 and 2) shows the titration curves of LCA in ethanol or methanol while NaOH is dissolved in the same alcohol; no extra singularities can be seen apart from the neutralization jump at the startup. By contrast, if LCA is dissolved in 20 mL of methanol (m_{LCA} = 0.2266 g, C_{LCA} = 1.43 wt %, n_{LCA} = 6 × 10^{-4} mol) and the titration achieved with an aqueous NaOH solution (T_{NaOH} = 0.02 M), the corresponding titration curve (Figure 10, curve 3) shows such singularities. This indicates that water is an essential ingredient to the fabrication of tubes through solvation reactions of the carboxylic groups.

Three plateaus can be discerned at pH = 6.1, 8.0, and 12.1. The pH curve stabilizes at pH $\approx$ 12.1, a value corresponding to that measured in EOC gels. The first plateau is assigned to the
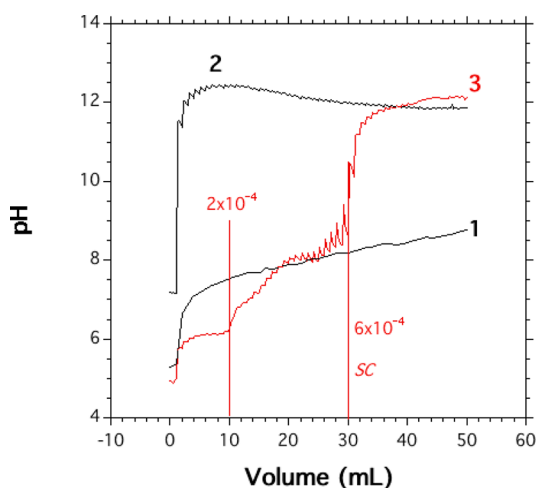
Figure 10. Titration curves. Curve 1: LCA in ethanol (C_{LCA} = 1 wt %) by NaOH in ethanol (T_{NaOH} = 0.01 M). Curve 2: 20 mL methanol by NaOH in ethanol (T_{NaOH} = 0.02 M). Curve 3: LCA in methanol (C_{LCA} = 1 wt %) by NaOH in water (T_{NaOH} = 0.02 M).

neutralization of the acidic function of LCA beyond which micellization occurs. Indeed, the pK_a of natural C_{24} bile acids is close to 5.1.[51] The second wave is a continuously increasing pH variation. It is speculated that micellar intermediates are generated during this step prior to the stoichiometric conditions of LCA neutralization (SC) being reached. Such a continuous micellization process has been previously reported in the class of bile acids as mentioned above. From the analysis of the present SAXS data, it can be speculated that SC samples contain helical ribbonlike species. The location of the SC point is shown in Figure 10 and corresponds to the onset of the third plateau for complete neutralization. At 1 wt %, the EOC conditions correspond to 6.8 times the stoichiometric conditions for neutralization, a very large excess of Na^+HO^- ions and water molecules. Figure 10 also shows that the pH is almost constant immediately beyond the SC threshold for stoichiometric neutralization. Previous cryo-TEM results have shown that thin fibrils are aggregating to form ribbons. Thus, it is reasonable to speculate that the domain of continuously increasing pH before SC in Figure 10 can correspond to such a bundling process, while the final closure of the helical ribbons into plain tubes does not correspond to a singularity in the titration curve. It can be identified only by separating the neutralization and ionic strength adjustment conditions, as in the AISC systems. Such a "cascade effect" in lithocholate systems is sensitive to the balance between the Cl^- and HO^- ions versus the Na^+ ion affecting the condensation degree of the counterion Na^+ onto the negatively charged carboxylate aggregates, their hydration degree, and specific H bonding.

CONCLUSION

The present data and analyses demonstrate that the preparation of lithocholate nanotubes can be performed either in an excess of sodium hydroxide aqueous solution or in stoichiometric conditions followed by an adjustment of the ionic strength by the addition of salt. High ionic strength and associated salt effects are first characterized by the flow properties of the gels, and creep-relaxation behaviors distinguish the systems. The SAXS data further characterize the morphological changes and the ordering of the cylindrical aggregates. It is suggested that species developed at low ionic strength and salt content (SC

systems) are loose helical ribbons in fresh systems. Once the systems have aged, intra- and interorderings develop resulting from electrostatic interactions between charged and exposed edges of the ribbons. A structural and organizational sequence is proposed to describe the time evolution of the "living" chiral species. Loose and disordered ribbons can self-organize upon aging into packets organized in a centered rectangular 2D symmetry. Upon further aging, the ribbons wrap more tightly around a cylinder of similar diameter than the final tubes. The exposed edges are now facing each other within the helical ribbons and their interordering is lost. At high ionic strengths (EOC systems) or salt content (AISC systems), the closure of the ribbons into plain tubes is effective. The strong enhancement of the VdW attractions that follows is responsible, in turn, for the onset of a high viscoelasticity typical of gels. Nevertheless, despite the fact that the elasticity of the networks in AISC and EOC gels is similar, the cohesiveness in AISC is diminished. Titration experiments reveal the specific role of water in hydration mechanisms of the carboxylate walls involved in the ribbons or tubes.

To conclude, De Gennes[13] described the closure of charged edges of a membrane into tubes. This first basic description was not supported by experimental evidence. Actually, his model was considering the case of bilayers presenting opposite charges at the edges of flat ribbons (no chirality). Here, we have identified ionic strength conditions where chirality is already expressed in the helical ribbons but their closure to tubes is not yet achieved. This last step is then triggered by the salt content which is reminiscent of the De Gennes description but with a *reverse consequence*. In conditions of large ionic strengths as used in the ordinary protocol, the twisting step goes to the closure since electrostatic repulsions of the chiral edges are screened. We believe that the situation in our systems despite being coincidental, as being related to the heterogeneous solid-liquid neutralization reaction in the micellization sequence, could be encountered in some other specific systems.

APPENDIX

Intermediate Ordering in SC Suspensions
After only 8 days, SC suspensions exhibit a complex SAXS curve with features different from those of the tubes in EOC samples.

It mixes form- and structure-factor scattering features. The first bump at Q = 0.01145 $Å^{-1}$ is representative of the cylindrical structure (diameter $2R$ = 660 Å) around which helical ribbons wind. Some of the diffraction peaks can be affected by the coincidence with form-factor oscillations. For instance, at Q = 0.0316, 0.0421, and 0.07 $Å^{-1}$ the features are clearly arising from the form-factor oscillations (red dotted vertical bars in Figure A1). Interestingly, the first five reflections at Q = 0.0183, 0.0285, 0.0390, 0.056, and 0.066 $Å^{-1}$ cannot be indexed according to a 2D hexagonal array of scatterers ($p6m$). The sequence of spacing is 1:1.5:2.1:3.0:3.6 instead of being $1:\sqrt{3}:2:\sqrt{7}:3$. This is noticeable as it is known that at higher concentrations, lithocholate tubes organize in a $p6m$ symmetry.[39] The arrangement is more likely a centered rectangular lattice, cmm plane group (eq A1).

$$Q_{hk} = 2\pi(h^2 a^{*2} + k^2 b^{*2})^{1/2} \qquad (A1)$$

with $h + k = 2n$. Q_{hk} is the reciprocal spacing for a reflection of indices h and k, and a^* and b^* are the dimensions of the reciprocal unit cell.
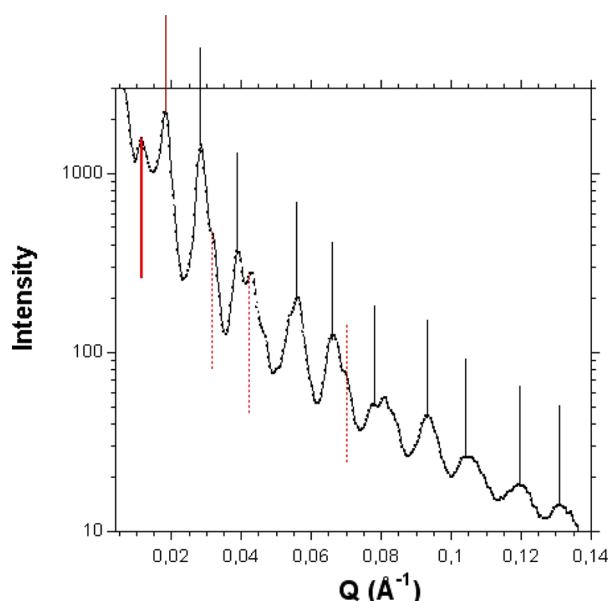
Figure A1. SAXS of a fresh SC system at C_{LCA} = 1% wt. Diffraction features are indexed according to a *cmm* 2D symmetry. Vertical bars are diffraction features taken into account in the indexation. Dotted vertical bars are form-factor features (see text).

Table A1 shows satisfactory agreement: all features can be indexed according to the *cmm* plane group with lattice parameters $b/a \approx 1/3$ and b = 687 Å, a = 224 Å (Q_{20}/Q_{02} = $a*/b*$ = 2.95).[52]

Table A1. Indexation of the Scattering Pattern in Figure A1 According to a Centered Rectangular *cmm* 2D Symmetry

experimental features (Å^{-1})	diffracting planes	experimental spacing sequence	theoretical spacing sequence	reference
0.0183	[02]	1	1	Q_{02}/Q_{02}
0.0285	[11]	1.56	1.56	Q_{11}/Q_{02}
0.039	[13], [04]	2.1	2.1	Q_{13}/Q_{02}
0.056	[22], [20]	3.1	3.1	Q_{22}/Q_{02}
0.066	[17]	3.6	3.8	Q_{17}/Q_{02}
0.078−0.0835	[31], [26]	4.4	4.6	Q_{31}/Q_{02}
0.0932	[35]	5.1	5.1	Q_{35}/Q_{02}
0.105	[40], [42]	5.7	5.9	Q_{40}/Q_{02}
0.119	[44]	6.5	6.2	Q_{44}/Q_{02}
0.131	[24], [51], [53]	7.1	7.1	Q_{24}/Q_{02}

These results suggest that loose (R = 330 Å) helical ribbons are first, strongly interacting in a rectangular arrangement (a = 224 Å, b = 687 Å).

ASSOCIATED CONTENT

Ⓢ Supporting Information
Viscosity of LCA aqueous suspensions, Creep recovery of a nearly SC system, and the effect of the length upon the SAXS profile for tubular species. This material is available free of charge via the Internet at http://pubs.acs.org.

AUTHOR INFORMATION

Corresponding Author
*E-mail: pierre.terech@cea.fr.

ADDITIONAL NOTES
[a]A creep-recovery experiment of a SC system would be technically not feasible due to its liquid character.
[b]Interestingly, the slight Q shift may not be interpreted as a slight reduction of the diameter but simply as the result of X-ray wave interference in a distance range of pitch values being similar to the tube diameter.

REFERENCES
(1) Schnur, J. M. *Science* **1993**, *262*, 1669.
(2) Schnur, J. M.; Price, R.; Schoen, P.; Yager, P. *Thin Solid Films* **1987**, *152*, 181.
(3) Schnur, J. M.; Shashidhar, R. *Adv. Mater.* **1994**, *6*, 971.
(4) Spector, M. S.; Price, R. R.; Schnur, J. M. *Adv. Mater.* **1999**, *11*, 337.
(5) Shimizu, T.; Masuda, M.; Minamikawa, H. *Chem. Rev.* **2005**, *105*, 1401.
(6) Iijima, S. *Nature* **1991**, *354*, 56.
(7) Hill, J. P.; Jin, W.; Kosaka, A.; Fukushima, T.; Ichihara, H.; Shimomura, T.; Ito, K.; Hashizume, T.; Ishii, N.; Aida, T. *Science* **2004**, *304*, 1481.
(8) Massey, J. A.; Power, K. N.; Winnik, M. A.; Manners, I. *Adv. Mater.* **1998**, *10*, 1559.
(9) Wang, X.-S.; Wang, H.; Coombs, N.; Winnik, M. A.; Manners, I. *J. Am. Chem. Soc.* **2005**, *127*, 8924.
(10) Mitchell, D. T.; Lee, S. B.; Trofin, L.; Li, N.; Nevanen, T. K.; Soderlund, H.; Martin, C. R. *J. Am. Chem. Soc.* **2002**, *124*, 11864.
(11) Selinger, J. V.; Spector, M. S.; Schnur, J. M. *J. Phys. Chem. B* **2001**, *105*, 7157.
(12) Chen, Z.; Majidi, C.; Srolovitz, D. J.; Haataja, M. *Appl. Phys. Lett.* **2011**, *98*, 011906.
(13) de Gennes, P.-G. *C. R. Acad. Sci. Paris* **1987**, *304*, 259.
(14) Lubensky, T. C.; Prost, J. *J. Phys. II* **1992**, *2*, 371.
(15) Chen, C. M. *Phys. Rev. E: Stat., Nonlinear, Soft Matter Phys.* **1999**, *59*, 6192.
(16) Chappell, J. S.; Yager, P. *Biophys. J.* **1991**, *60*, 952.
(17) Oda, R.; Huc, I.; Schmutz, M.; Candau, S. J.; MacKintosh, F. C. *Nature* **1999**, *399*, 566.
(18) Brizard, A.; Aimé, C.; Labrot, T.; Huc, I.; Berthier, D.; Artzner, F.; Desbat, B.; Oda, R. *J. Am. Chem. Soc.* **2007**, *129*, 3754.
(19) Terech, P.; de Geyer, A.; Struth, B.; Talmon, Y. *Adv. Mater.* **2002**, *14*, 495.
(20) Jean, B.; Oss-Ronen, L.; Terech, P.; Talmon, Y. *Adv. Mater.* **2005**, *17*, 728.
(21) *Molecular Gels: Materials with Self-Assembled Fibrillar Networks*; Weiss, R. G., Terech, P., Eds.; Springer: Dordrecht, The Netherlands, 2006, pp 976.
(22) Zhang, X.; Zou, J.; Tamhane, K.; Kobzeff, F. F.; Fang, J. *Small* **2010**, *6*, 217.
(23) Lee, S. J.; Kim, E.; Seo, M. L.; Do, Y.; Lee, Y.-A.; Lee, S. S.; Jung, J. H.; Kogiso, M.; Shimizu, T. *Tetrahedron* **2008**, *64*, 1301.
(24) Pouget, E.; Fay, N.; Dujardin, E.; Jamin, N.; Berthault, P.; Perrin, L.; Pandit, A.; Rose, T.; Valéry, C.; Thomas, D.; Paternostre, M.; Artzner, F. *J. Am. Chem. Soc.* **2010**, *132*, 4230.
(25) Ziserman, L.; Lee, H.-Y.; Raghavan, S. R.; Mor, A.; Danino, D. *J. Am. Chem. Soc.* **2011**, *133*, 2511.

(26) Arora, S. K.; Germain, G.; Declercq, J. P. *Acta Crystallogr.* **1976**, *32*, 415.

(27) Pernot, P.; Theveneau, P.; Giraud, T. *J. Phys.: Conf. Ser.* **2010**, 012009.

(28) Berne, B. J.; Pecora, R. *Dynamic Light Scattering with Applications to Chemistry, Biology and Physics*; Dover Publications, Inc.: New York, 2000.

(29) Terech, P.; Friol, S.; Sangeetha, N.; Talmon, Y.; Maitra, U. *Rheol. Acta* **2006**, *45*, 435.

(30) Talmon, Y.; Schmidt, J.; Terech, P. Cryogenic Temperature Transmission Electron Microscopy Study of Self-Aggregation of Sodium Lithocholate Single-Molecular Walled Nanotubes. In *Mesoscale Phenomena in Fluid Systems*; Case, F., Alexandridis, P., Eds.; ACS Symposium Series 861; American Chemical Society: Washington, DC, 2003; p 17.

(31) Terech, P.; Talmon, Y. *Langmuir* **2002**, *18*, 7240.

(32) Zarras, P.; Vogl, O. *Prog. Polym. Sci.* **1999**, *24*, 485.

(33) O'Connor, C. J.; Wallace, R. G. *Adv. Colloid Interface Sci.* **1985**, *22*, 1.

(34) Carey, M. C. *Hepatology* **1984**, *4*, 66S.

(35) O'Connor, C. J.; Ch'ng, B. T.; Wallace, R. G. *J. Colloid Interface Sci.* **1983**, *95*, 410.

(36) Blow, D. M.; Rich, A. *J. Am. Chem. Soc.* **1960**, *82*, 3566.

(37) Rich, A.; Blow, D. M. *Nature* **1958**, *46*, 423.

(38) Sobotka, H.; Czeczowiczka, N. *J. Colloid Sci.* **1958**, *13*, 188.

(39) Terech, P.; Jean, B.; Ne, F. *Adv. Mater.* **2006**, *18*, 1571.

(40) Tschoegl, N. W. *The Phenomenological Theory of Linear Viscoelastic Behavior*; Springer-Verlag: Berlin, 1989.

(41) Larson, R. G. *The Structure and Rheology of Complex Fluids*; Oxford University Press: New York, 1999.

(42) Pusey, P. N.; Van Megan, W. *Phys. A (Amsterdam, Neth)* **1989**, *157*, 705.

(43) Provencher, S. W. *Comput. Phys. Commun.* **1982**, *27*, 213.

(44) Talmon, Y. Cryogenic Temperature Transmission Electron Microscopy in the Study of Surfactant Systems. In *Modern Characterization Methods of Surfactant Systems*; Binks, B. P., Ed.; Marcel Dekker: New York, 1999; p 147.

(45) Nyrkova, I. A.; Semenov, A. N.; Aggeli, A.; Bell, M.; Boden, N.; McLeish, T. C. B. *Eur. Phys. J.* **2000**, *B 17*, 499.

(46) Vainshtein, B. K. *Diffraction of X-rays by Chain Molecules*; Elsevier: Amsterdam, 1966.

(47) Hamley, I. W. *Macromolecules* **2008**, *41*, 8948.

(48) Pringle, O. A.; Schmidt, P. W. *J. Appl. Crystallogr.* **1971**, *4*, 290.

(49) Terech, P.; Ramasseul, R.; Volino, F. *J. Phys. (Paris)* **1985**, *46*, 895.

(50) Teixeira, C. V.; Amenitsch, H.; Fukushima, T.; Hill, J. P.; Jin, W.; Aida, T.; Hotokka, M.; Linden, M. *J. Appl. Crystallogr.* **2010**, *43*, 850.

(51) Hofmann, A. F.; Mysels, K. J. *J. Lipid Res.* **1992**, *33*, 617.

(52) Hendrikx, Y.; Charvolin, J. *Liq. Cryst.* **1992**, *11*, 677.